RSC Advances

RSC Publishing

COMMUNICATION

View Article Online
View Journal | View Issue

Acetylene black derived hollow carbon nanostructure and its application in lithium–sulfur batteries†

Cite this: *RSC Advances*, 2013, **3**, 16936

Received 7th June 2013,
Accepted 24th July 2013

DOI: 10.1039/c3ra42835d

www.rsc.org/advances

Jingjing Tang, Juan Yang and Xiangyang Zhou*

Acetylene black derived hollow carbon nanostructure (HCS) with a unique hollow inner cavity was prepared by a facile one-pot acid steaming method. By evaluating its electrochemical performance, the obtained HCS–S was demonstrated to be a suitable cathode material for lithium–sulfur batteries.

Lithium-ion batteries have attracted increasing attention in recent years due to the inescapable exhaustion of fossil fuels and environmental issues.[1] However, the high cost, safety concerns, and the relatively low capacity of intercalation cathode materials impede their use in some particular applications such as electric vehicles and large scale energy storage systems.[2] Developing alternative low cost, abundant electrode materials with high energy and power density is critical for the wide use of rechargeable batteries for transportation. In recent years, considerable efforts have been devoted to the development of lithium–sulfur (Li-S) batteries, ascribed to the ultra high theoretical specific capacity of elemental sulfur (1673 mAh g^{-1}) at a moderate voltage of 2.2 V *vs.* Li/Li^+, and its extremely low cost and widespread availability, which make it a promising candidate for cathode materials.[3,4] Nevertheless, the Li-S cell is plagued with problems that have hindered its large-scale practical application. The low electrical conductivity of sulfur limits its utilization as an active material as a result of poor electrochemical contacts within the material. Another drawback is the diffusion of lithium polysulfides (Li_2S_n, the sulfur reduction products) into the electrolyte solution and reactions with the negative lithium electrodes. The continuous reduction of the Li_2S_n by the Li anodes prevents their reoxidation back to elemental sulfur at the cathode side upon charging, which is known as the "shuttle" phenomenon of Li-S batteries, and leads to a decreased utilization of the overall active material mass during discharge, current leakage, poor cyclability, and reduced coulombic efficiency of the battery.[5,6]

Significant efforts have been made to address the polysulfide dissolution and shuttling issues in Li-S secondary batteries.[7–9] One of the most effective methods is to confine sulfur in carbon hosts with satisfactory electronic conductivity, such as porous carbon spheres and hollow structures, which can suppress the outward diffusion of lithium polysulfides.[10,11] Concerning hollow carbon nanostructures (HCS), various strategies have been attempted in recent years to realize the specific hollow structures, such as self-assembly, spray-drying, and template synthesis.[12–14] Among them, the template approach is a common synthetic strategy to fabricate HCS by employing sacrificial templates, such as silica and anodic aluminium oxide templates.[15,16] Although it is an efficient way to obtain homogeneous hollow structures, the template method is time consuming and involves multi-step preparation. As for the synthesis of C–S composites, vapor phase infusion and melt-diffusion are the most widely used strategies which could realize sublimed sulfur impregnation into carbon hosts.[7,10]

Herein, we provide a novel approach to realize the facile synthesis of HCS *via* a one-pot acid steaming process. Pristine acetylene black (p-AB) was sealed in a Teflon vessel in the presence of HNO_3 solution. HCS was obtained with the aid of acid steaming at a temperature of 150 °C. Additionally, a new route for the preparation of C–S composites was proposed. Instead of the conventional vapor phase infusion and melt-diffusion strategy, a hydrothermal reaction was used to generate sulfur in and around the as-prepared HCS. The detailed experimental section is available in the ESI.†

The received p-AB is composed of cross-linked carbon nanospheres with an average diameter of 50 nm (Fig. 1a and b). After the acid steaming process, the apparent morphology of the carbon nanospheres is mostly maintained (Fig. 1c). However, an obvious change took place in the inner structure of these nanoparticles. It can be seen from Fig. 1b that p-AB is composed of agglomerated carbon nanospheres and formed a specific steric chain structure. Experiments demonstrate that after the acid steaming treatment, p-AB was oxidized and the inner graphite layers tended to be consumed by the acid steam, forming the final cross-linked hollow nanostructure with a thick shell of 8–12 nm (Fig. 1d and insert). Fig. 1e shows a simplified schematic illustration of the synthesis

School of Metallurgy and Environment, Central South University, Lushan South Road 932, Changsha, China. E-mail: hncsyjy308@163.com; Fax: +86 731 8871017; Tel: +86 731 88836329

† Electronic supplementary information (ESI) available: Detailed synthesis procedure and material characterization, electrochemical tests. See DOI: 10.1039/c3ra42835d

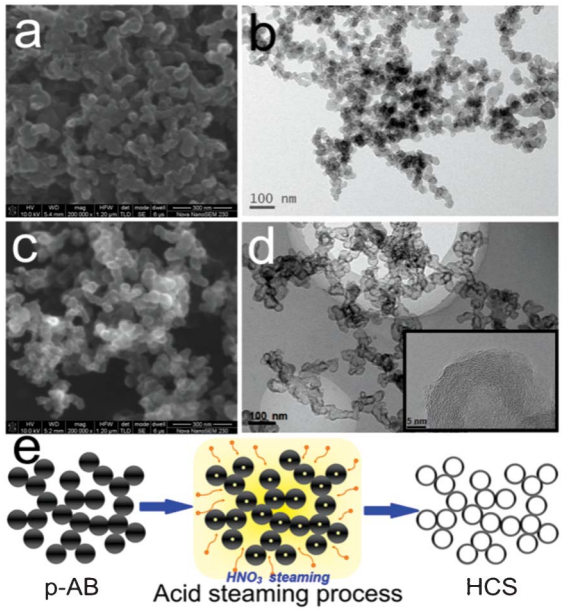

Fig. 1 SEM images of (a) p-AB and (c) HCS. TEM images of (b) p-AB and (d) HCS. The insert in (d) is the HRTEM image of HCS. (e) Simplified schematic illustration of the synthesis process for HCS.

process, which is proven to be an effective and facile way to obtain HCS. The HRTEM image of the HCS shown in the insert of Fig. 1d demonstrated the concentric turbostratic shells of HCS.

The crystallinity of samples was determined by X-ray diffraction (XRD). As shown in Fig. 2a, the peak at $2\theta = 25^\circ$ can be ascribed to the (002) reflection of carbon. There is a subsidiary broad peak centered at 43° due to the indistinguishability of the (100) and (101) peaks, which is a reflection of the disordered structure. However, after the acid steaming, the (002) peak became sharper and more intense. The parameters of the samples derived from the XRD data are reported in Table S1 (see ESI†). Compared with p-AB, HCS has a smaller d_{002} value and a larger crystallite size (L_c), suggesting that the acid steaming process promoted the formation of a more graphitic carbon structure. Meanwhile, the sulfur in the HCS–S composite exists in a crystallized form. To better understand the interactions between sulfur and carbon, the structures of the samples were characterized using Raman spectroscopy as shown in Fig. 2b. Both p-AB and HCS exhibit two peaks at approximately 1353 and 1583 cm^{-1}, corresponding to the D band and G band, respectively. The D band comes from structural defects and disorder-induced features of carbon, while the G band corresponds to the stretching vibration mode of the graphite crystals.[17] The peak integrated intensity ratios of the D band to the G band (I_D/I_G) for p-AB and HCS are estimated to be 1.56 and 1.4, indicating that there are more disordered defective carbons in p-AB. However, no obvious difference was detected between HCS and HCS–S. It is noteworthy that the electrical conductivity of graphitic carbon is substantially higher than that of absolute amorphous carbon. Even partially graphitized carbon materials are attractive, which is ascribed to the favourable transport of electrons from partially graphitized carbon to sulfur, improving the electrochemical stability of the C–S composites.

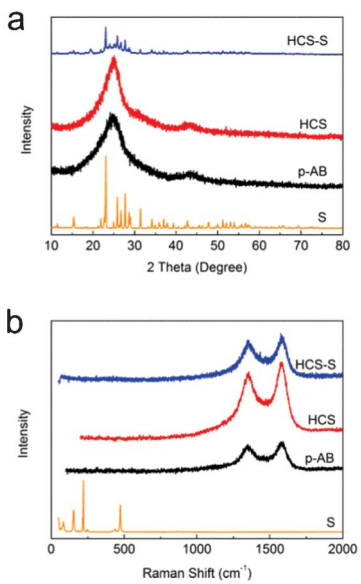

Fig. 2 (a) XRD patterns and (b) Raman spectra of the samples.

For further characterization, Fourier transform infrared spectroscopy (FT-IR) and X-ray photoelectron spectroscopy (XPS) were also performed. The FT-IR spectra of p-AB and HCS presented in Fig. S1 (ESI†) reveal the molecular structure changes induced by the acid steaming. For both p-AB and HCS, three common peaks located at about 3430, 1620 and 606 cm^{-1} are ascribed to the O–H, C–C and C–H functional groups, respectively.[18,19] Compared with the peaks of p-AB, another three peaks appearing at 1730, 1383 and 1250 cm^{-1} are also detected in HCS, which are assigned to the oscillation of carboxylic groups (COOH), O–H bending deformation in carboxylic acid groups, and C–O–C vibrations, respectively.[20,21] These results demonstrate that after the acid steaming process, the final product displays a uniform hollow structure with abundant carboxyl acid groups on the surface, which will make it easier to induce a series of chemical reactions to retain foreign materials along the interface. Fig. S2 (ESI†) shows the deconvolution of the C 1s regions of the XPS spectra for the identification of surface functionalities, and after fitting with several component peaks, four types of carbon functional groups (C=C at 284.5–284.8 eV, C–C at 285.6–286.1 eV, C–O at 286.6–287.1 eV, and O–C=O at 288.7–289.1 eV) can be assigned.[22,23] The C 1s spectrum of p-AB (Fig. S2a, ESI†) could be deconvoluted into three peaks, which correspond to carbon sp^2 (C=C), carbon sp^3 (C–C) and hydroxyl groups (C–O). However, carboxylates (O–C=O) are detected in the HCS sample as shown in Fig. S2b (ESI†), which further confirms that a large number of carboxylic groups have been generated on the surface of the HCS after acid steaming.

To demonstrate the possible structural advantages of HCS, a HCS–S composite obtained by a hydrothermal process was tested as a cathode for Li-S batteries. The p-AB–S composite was also prepared for comparison. The electrochemical reaction mechanism of the HCS–S cathode was revealed using cyclic voltammetry (CV). The CV scan was performed on the HCS–S cathode between

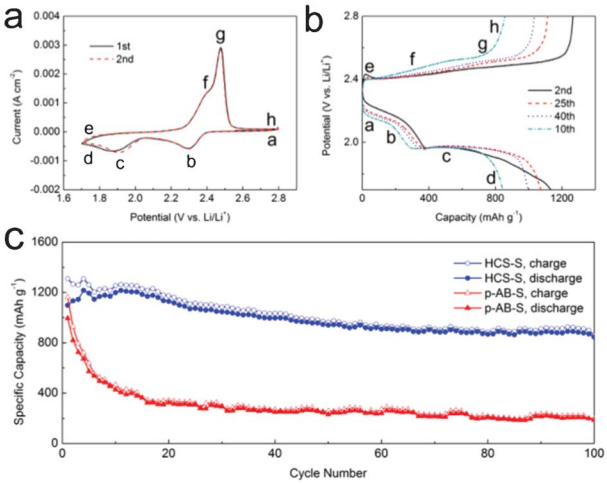

Fig. 3 (a) Typical CV curves at a sweep rate of 0.1 mV s^{-1}. (b) Typical voltage *vs.* capacity profiles of the HCS–S composite at a current density of 200 mA g^{-1}. (c) Cycling performance of HCS–S and p-AB–S.

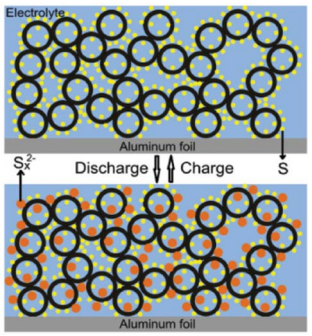

Fig. 4 Model illustration of the discharge/charge process of the HCS–S cathode material for Li-S batteries. The yellow circles and red circles represent sulfur and polysulfide, respectively.

2.8 and 1.7 V using a 0.1 mV s^{-1} scan rate. As shown in Fig. 3a, a pair of redox peaks indicates that during the discharging/charging process, the electrochemical reduction and oxidation of sulfur occurs in two stages. The first peak at 2.3 V involves the reduction of elemental sulfur to lithium polysulfide. The second peak at 1.8–2.0 V involves the reduction of lithium polysulfide to Li_2S_2 and eventually to Li_2S. The oxidation peak at 2.4 V is associated with the formation of Li_2S_n. This process continues until lithium polysulfide is completely consumed to produce sulfur at 2.48 V.[11,24]

Fig. 3b and c show the typical galvanostatic discharge/charge profiles of HCS–S, and the cycling performance of HCS–S and p-AB–S, respectively. Specific capacity values were calculated based on the mass of sulfur. As shown in Fig. S3 (ESI†), the sulfur content in the HCS–S composite was determined by TGA to be approximately 57% (after taking a 7% mass ratio of the carboxyl functional groups). It is apparent from Fig. 3b that the discharge/charge voltage plateaus were generally in accordance with the redox peaks observed in the CV scans. The HCS–S composite showed a high discharge capacity of 1133 mAh g^{-1} in the second cycle, and good capacity retention. Fig. 3c shows the cycling performance of the HCS–S and p-AB–S composites. At a constant current density of 200 mA g^{-1}, the initial discharge capacities of p-AB–S and HCS–S are 995 and 1098 mAh g^{-1}, respectively. However, the HCS–S composite showed much better cycling stability, with a reversible capacity of 844 mAh g^{-1} after 100 cycles. In contrast, the discharge capacity of p-AB–S steadily dropped to 186 mAh g^{-1} by the 100th cycle, which was less than 25% of the value for HCS–S. The superior electrochemical property of HCS-S could be explained by the model illustration in Fig. 4. It is known that acetylene black is an industrially manufactured carbon material composed of spheres and their fused aggregates. With the aid of acid steaming, the obtained product takes on a cross-linked "bead-like" structure, which consists of aggregated hollow nanospheres with a partially graphitized nature. Additionally, after the oxidation process, a large number of carboxylic groups were generated on the surface of HCS. According to previous reports, the functional groups of the carbonaceous surface could provide a chemical gradient which favours the retardation of the diffusion of lithium polysulfides out of the electrode, thus facilitating more complete redox reactions for an acceptable reversible capacity.[4,25]

Conclusions

HCS was synthesized *via* a novel one-pot acid steaming process. The obtained sample is composed of cross-linked hollow carbon nanospheres with abundant carboxylic groups on their surface. This method is simple, effective and easily scaled up. In addition, a hydrothermal strategy was proposed to realize the synthesis of a HCS–S composite. When evaluating the electrochemical performance, HCS shows outstanding performance as a sulfur host material for high capacity cathodes for use in Li-S batteries. When the sulfur content was up to 57 wt%, HCS–S shows an initial discharge capacity of 1098 mAh g^{-1}, and the capacity retention is as high as 77% at the 100th cycle, which demonstrates the stable cycling performance. The superior electrochemical properties of the HCS–S composite can probably be attributed to the novel hollow carbon structure and the proposed hydrothermal strategy to synthesize the C–S composite.

Acknowledgements

This work was financially supported by the National Natural Science Foundation of China (grant no. 51204209 and 51274240) and Hunan Provincial Innovation Foundation for Postgraduate.

References

1 J. W. Fergus, *J. Power Sources*, 2010, **195**, 393.
2 J. M. Tarascon and M. Armand, *Nature*, 2001, **414**, 359.
3 J. Guo, Y. Xu and C. Wang, *Nano Lett.*, 2011, **11**, 4288.
4 X. Ji, K. T. Lee and L. F. Nazar, *Nat. Mater.*, 2009, **8**, 500.
5 X. Liang, Z. Wen, Y. Liu, H. Zhang, J. Jin, M. Wu and X. Wu, *J. Power Sources*, 2012, **206**, 409.
6 Y. Yang, G. Zheng, S. Misra, J. Nelso, M. F. Toney and Y. Cui, *J. Am. Chem. Soc.*, 2012, **134**, 15387.

7 C. Zhang, H. B. Wu, C. Yuan, Z. Guo and X. W. Lou, *Angew. Chem., Int. Ed.*, 2012, **51**, 9592.
8 X. Tao, X. Chen, Y. Xia, H. Huang, Y. Gan, R. Wu, F. Chen and W. Zhang, *J. Mater. Chem. A*, 2013, **1**, 3295.
9 Y. Fu and A. Manthiram, *RSC Adv.*, 2012, **2**, 5927.
10 J. Schuster, G. He, B. Mandlmeier, T. Yim, K. T. Lee, T. Bein and L. F. Nazar, *Angew. Chem., Int. Ed.*, 2012, **51**, 3591.
11 N. Jayaprakash, J. Shen, S. S. Moganty, A. Corona and L. A. Archer, *Angew. Chem., Int. Ed.*, 2011, **50**, 5904.
12 J. Cao, Y. Wang, P. Xiao, Y. Chen, Y. Zhou, J. H. Ouyang and D. Jia, *Carbon*, 2013, **56**, 389.
13 A. C. Sanchez, I. Imaz, M. C. Sarabia and D. Maspoch, *Nat. Chem.*, 2013, **5**, 203.
14 X. Zhao, J. Zhu, W. Cai, M. Xiao, L. Liang, C. Liu and W. Xing, *RSC Adv.*, 2013, **3**, 1763.
15 N. Brun, K. Sakaushi, L. Yu, L. Giebeler, J. Eckert and M. M. Titirici, *Phys. Chem. Chem. Phys.*, 2013, **15**, 6080.
16 G. Zheng, Y. Yang, J. J. Cha, S. S. Hong and Y. Cui, *Nano Lett.*, 2011, **11**, 4462.
17 C. Kim, S. H. Park, J. I. Cho, D. Y. Lee, T. J. Park, W. J. Lee and K. S. Yang, *J. Raman Spectrosc.*, 2004, **35**, 928.
18 H. Wang, Q. Hao, X. Yang, L. Lu and X. Wang, *Electrochem. Commun.*, 2009, **11**, 1158.
19 V. Gomez-Serrano, F. Piriz-Almeida, C. J. Duran-Valle and J. Pastor-Villegas, *Carbon*, 1999, **37**, 1517.
20 S. Goyanes, G. R. Rubiolo, A. Salazar, A. Jimeno, M. A. Corcuera and I. Mondragon, *Diamond Relat. Mater.*, 2007, **16**, 412.
21 Y. Z. Jin, C. Gao, W. K. Hsu, Y. Zhu, A. Huczko, M. Bystrzejewski, M. Roe, C. Y. Lee, S. Acquah, H. Kroto and D. R. M. Walton, *Carbon*, 2005, **43**, 1944.
22 L. Zhuo, Y. Wu, J. Ming, L. Wang, Y. Yu, X. Zhang and F. Zhao, *J. Mater. Chem. A*, 2013, **1**, 1141.
23 M. L. Sham and J. K. Kim, *Carbon*, 2006, **44**, 768.
24 J. Chen, Q. Zhang, Y. Shi, L. Qin, Y. Cao, M. Zheng and Q. Dong, *Phys. Chem. Chem. Phys.*, 2012, **14**, 5376.
25 V. S. Kolosnitsyn and E. V. Karaseva, *Russ. J. Electrochem.*, 2008, **44**, 506.